Available online at www.sciencedirect.com
SCIENCE DIRECT®
PERGAMON
International Journal of Heat and Mass Transfer 46 (2003) 3991–4001
International Journal of HEAT and MASS TRANSFER
www.elsevier.com/locate/ijhmt

Measurements of wall heat (mass) transfer for flow through blockages with round and square holes in a wide rectangular channel

S.C. Lau [a,*], J. Cervantes [a], J.C. Han [a], R.J. Rudolph [b], K. Flannery [b]

[a] Department of Mechanical Engineering, Texas A&M University, College Station, TX 77843-3123, USA
[b] Siemens-Westinghouse Power Company, 2151 Alternate A1A South, Jupiter, FL 33477, USA

Received 25 October 2002; received in revised form 2 May 2003

Abstract

Naphthalene sublimation experiments were conducted to study heat (mass) transfer enhancement by blockages with staggered round and square holes for turbulent air flows through a wide rectangular channel. The blockages and the channel had the same cross-section. The results showed that the blockages enhanced the average heat (mass) transfer on the channel walls by 4.7–6.3 times that for fully developed turbulent flow through a smooth channel. The blockages with round holes enhanced more heat (mass) transfer on the channel walls but caused larger pressure drops than the blockages with square holes, which had a 27% larger flow cross-sectional area.

Keywords: Turbulent flow; Naphthalene sublimation; Mass transfer; Blockages with holes

1. Introduction

To enable gas turbine engines to operate at very high temperatures, air from the compressors is used to cool the airfoils on the stators and the rotors. The cooling air removes heat from the airfoil walls as it flows through internal shaped passages with turbulators and/or pin fins, and/or as it impinges on the inside surfaces of the airfoil walls near the leading edges. The cooling air then exits the airfoils through strategically located arrays of film cooling holes along both the pressure and suction walls of the airfoils, holes at the tips of the airfoils, and slots along the trailing edges. In a recent design concept for cooling the pressure and suction walls near the trailing edge of an airfoil, cooling air is forced to flow through parallel blockages with staggered holes before it exits the airfoil through the trailing edge slots. Each of these blockages has the same cross section as the flow cross section between the pressure and suction walls near the airfoil trailing edge. After passing through the holes along a blockage, the cooling air impinges onto the next blockage and is deflected toward the suction and pressure walls of the airfoil before it finally passes through the staggered holes along the next blockage. These blockages cause vigorous mixing of the flow and may significantly enhance the heat transfer from the walls of the airfoil to the cooling air.

In this experimental study, we examine the heat transfer characteristics of flows through these blockages with staggered holes. The tail region of an airfoil with these blockages is modeled as a rectangular channel in which air flows through an array of staggered holes in four blockages that have the same cross section as the rectangular channel. We conduct naphthalene sublimation experiments to determine the overall mass transfer coefficients and the distributions of the local mass transfer coefficient on the walls between blockages, for blockages with round holes and square holes with rounded corners, and for four mass flow rates corresponding to Reynolds numbers (based on the channel hydraulic diameter) of about 7000, 14,000, 21,000, and 28,000. We use the analogy between heat transfer and

* Corresponding author.

0017-9310/03/$ - see front matter
doi:10.1016/S0017-9310(03)00246-1

Nomenclature

A_c	flow cross-sectional area of test channel, m^2
A_s	surface area, m^2
D_h	hydraulic diameter of test channel, m
f	friction factor
f_0	reference friction factor for fully developed turbulent flow in smooth channel
h_m	local mass transfer coefficient, m/s
$\bar{h}_m$	average mass transfer coefficient, m/s
$\dot{m}$	air mass flow rate, kg/s
$\dot{M}_n$	rate of total mass transfer from upstream naphthalene surfaces, kg/s
$\dot{M}''_n$	local naphthalene mass flux, kg/(m^2 s)
Nu_{D_h}	local Nusselt number
$\overline{Nu}_{D_h}$	average Nusselt number
Nu_0	reference Nusselt number for fully developed turbulent flow in smooth channel
p	pressure, N/m^2
$p_{v,w}$	vapor pressure on naphthalene surface, N/m^2
P	perimeter of test channel, m
Pr	Prandtl number
R	gas constant of naphthalene vapor, kJ/(kg K)
Re_{D_h}	Reynolds number
Sc	Schmidt number
Sh_{D_h}	local Sherwood number
$\overline{Sh}_{D_h}$	average Sherwood number
Sh_0	reference Sherwood number for fully developed turbulent flow in smooth channel
T	temperature, K
TP	thermal performance ratio, defined as $(\overline{Nu}_{D_h}/Nu_0)(f/f_0)^{-1/3}$
T_w	surface temperature, K
$\dot{V}$	volumetric flow rate of air, m^3/s
$\overline{V}$	average velocity, m/s

Greek symbols

ΔM_n	total mass transfer from naphthalene surface to air, kg
$\Delta p/\Delta x$	pressure gradient across two successive blockages, N/m^2
Δt	duration of experiment, s
Δz	local change of elevation on naphthalene surface, m
μ	dynamic viscosity of air, N s/m^2
ρ	density of air, kg/m^3
$\rho_{v,b}$	local bulk vapor density of naphthalene, kg/m^3
$\bar{\rho}_{v,b}$	average bulk vapor density of naphthalene, kg/m^3
ρ_s	density of solid naphthalene, kg/m^3
$\rho_{v,w}$	vapor density of naphthalene on naphthalene surface, kg/m^3
σ	mass diffusion coefficient of naphthalene vapor in air, m^2/s

mass transfer to relate the experimentally determined mass transfer enhancement to heat transfer enhancement. The naphthalene coated and mass transfer inactive surfaces in this study are analogous to isothermal and adiabatic surfaces, respectively, in corresponding heat transfer experiments. In addition, we measure the pressure drops caused by these blockages in the rectangular channel.

Detailed surveys of published studies on internal cooling of gas turbine airfoils have been presented in Han et al. [1] and Lau [2]. Many researchers have studied heat transfer enhancement in channels with turbulence promoters, pin fins, and impinging jets, with and without rotation. There have been a number of studies of heat transfer for turbulent flows through channels with perforated ribs or ribs with various openings for flows to pass through, such as Kukreja and Lau [3], Hwang et al. [4], Liou and Chen [5], and Buchlin [6]. Kukreja and Lau [3] conducted experiments using the transient liquid crystal technique to measure the local heat transfer distributions for turbulent flows through a square channel with solid and perforated ribs on two opposite walls. They presented detailed distributions of the local heat transfer coefficient between solid ribs and perforated ribs. The experimental results showed that perforated ribs enhanced less overall heat transfer than solid ribs. Perforated ribs caused lower pressure drop than solid ribs, but replacing solid ribs with perforated ribs did not improve thermal performance. Increasing the size of the holes, the number of holes, or the total hole area did not increase the overall heat transfer. Buchlin [6] tested five types of perforated ribs: bottom hole type, tilted hole type, arch type, column type, and chevron type. He observed an increase of the local heat transfer immediately downstream of the perforated ribs, when compared with corresponding local heat transfer for solid ribs, and recommended an optimal design with chevron type perforated ribs. Whereas the ribs in these prior studies had cross sections much smaller than the cross sections of the flow channels, with rib heights typically less than or about one-sixth of the channel heights, the blockages in the present study have the same cross section as the cross section of the rectangular channel.

Moon and Lau [7] conducted experiments with thermochromic liquid crystals to study heat transfer between two blockages with holes and pressure drops across the blockages, for turbulent air flows in a rectangular channel. They obtained the average heat transfer coefficients and the local heat transfer distributions on one of the channel walls between two blockages, and the overall pressure drops across the blockages, for nine different staggered arrays of holes in the blockages and two Reynolds numbers. For the hole configurations studied, the blockages enhanced heat transfer by about five to eight times, but significantly increased the pressure drop. Smaller holes in the blockages caused higher heat transfer enhancement but larger increase of the pressure drop than larger holes. Because of the large pressure drop, the heat transfer per unit pumping power was lower with the blockages than without them. The local heat transfer was the lowest immediately downstream of the holes in the upstream blockage, the highest upstream of the downstream blockage, and also relatively high in regions of reattachment of the jets leaving the upstream holes. The local heat transfer distribution was strongly dependent on the configuration of the hole array in the blockages. Except for Moon and Lau [7], there has not been any other study of heat transfer for flow through blockages with holes in a channel, with the cross section of the blockages the same as the cross section of the channel.

2. Experimental apparatus and instrumentation

The test apparatus for this study is an open flow loop in an air-conditioned laboratory. As shown in Fig. 1, the main components of the open flow loop are the test section, a plenum, a calibrated orifice flow meter, a gate valve, and a blower. During an experiment, air at about 22 °C is drawn through the test section. Upon exiting the flow loop, the air is ducted to the outside of the laboratory.

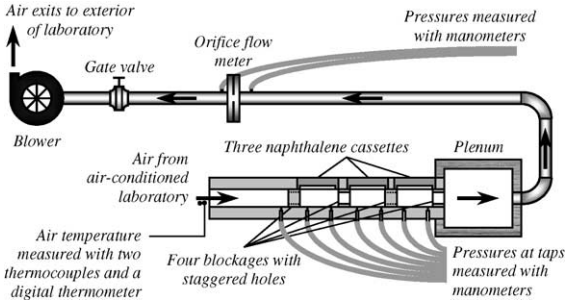

Fig. 1. Schematic of test apparatus for mass transfer and pressure measurement experiments.

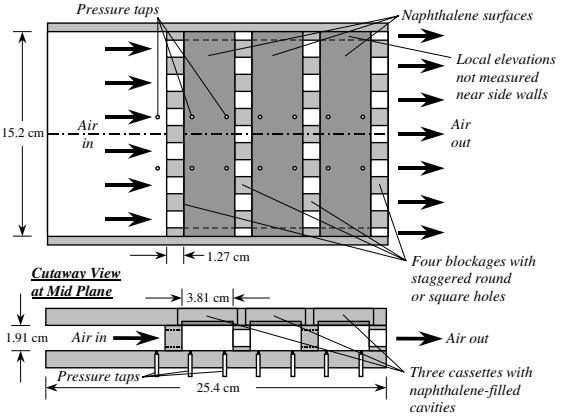

Fig. 2. Schematic of test channel with blockages and naphthalene-coated surfaces on top wall between blockages.

The test section is a 25.4-cm long rectangular channel with a flow cross section of 15.2 cm (width) by 1.91 cm (height), which gives an aspect ratio of 8:1. The four walls of the test channel are constructed entirely of aluminum. Inside the channel, there are four aluminum blockages, each with six equally spaced round holes or square holes with rounded corners. These blockages have a thickness of 1.27 cm and the same cross section as the channel cross section, as shown in Fig. 2. The first blockage is 8.89 cm from the channel entrance, and the distance between successive blockages is 3.81 cm, which is two times the height of the blockages or the channel. To promote mixing of the flow between blockages, the hole array is staggered. Fig. 3 gives the detailed dimensions of the blockages and the holes. The diameter of the round holes and the height (and the width) of the square holes are both 1.27 cm, while the center-to-center distance between adjacent holes is 2.54 cm. The rounded

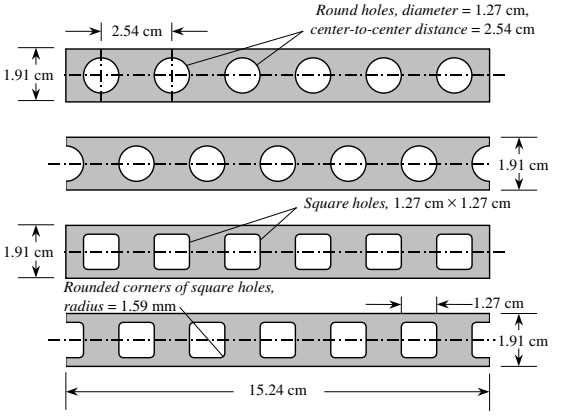

Fig. 3. Dimensions and configurations of blockages with round and square holes.

corners of the square holes have a radius of 1.59 mm. Based on these dimensions, it may be shown that the ratios of the total hole cross-sectional area to the channel cross-sectional area, for the blockages with round and square holes, are 26.2% and 33.2%, respectively.

To facilitate measurements of the local and overall mass transfer coefficients on the principal walls between blockages, three aluminum cassettes are inserted into slots in the top wall (see Fig. 2). Each cassette has a 3.18-mm deep cavity with a 3.18-mm thick rim. The cavity is filled with naphthalene during a casting process, exposing a smooth flat naphthalene surface. The naphthalene surface measures 3.81 cm × 15.24 cm, the dimensions of the surface of the top wall between blockages. As shown in Fig. 2, the rim of each cassette rests on top of the blockages and the side walls so that the entire surface of the top wall between two blockages is a naphthalene surface. Also, the cassettes are designed such that they may be quickly inserted into the slots in the top wall or removed for measurements. Adhesive tape is used to prevent air leakage between the cassettes and the channel walls during an experiment.

The mass flow rate of air through the test section and the flow loop is controlled with the gate valve. The pressure drop across the orifice and the pressure upstream of the orifice are measured with an inclined manometer and a U-tube manometer, respectively. The pressures at the orifice flow meter are needed to calculate the air mass flow rate. The temperature of the air is measured with two thermocouples whose junctions are located at the entrance of the test section, and a digital multi-channel thermometer with a resolution of 0.1 °C. The thermocouples and the digital thermometer are calibrated with a constant temperature bath and an NIST calibrated mercury thermometer. The duration of an experiment is measured with a digital stopwatch that has a resolution of 0.01 s.

To obtain the average mass transfer coefficients, the naphthalene cassettes are weighed one at a time with a Sartorius electronic balance before and after each test run. The electronic balance has a range of 0.0–160.0 g and a resolution of 0.1 mg. To determine the local mass transfer distributions, the elevations at a grid of 2457 points (27 × 91) on the naphthalene surface and on the top surface of the rim of each cassette are measured with a Starrett electronic depth gauge before and after each test run. The depth gauge has a lever-type LVDT head, a range of ±0.2 mm, and a resolution of 0.0002 mm. The elevation measurements on the top surface of the rim are needed to determine the location of the reference plane of the naphthalene surface in the calculations of the elevation changes at the grid points on the naphthalene surface.

Fourteen pressure taps are installed on the bottom wall for determining the pressure drops across the blockages at the holes and between the holes, as shown in Fig. 2. These taps are located 6.35 mm upstream and downstream of the blockages. Two additional pressure taps are located on one of the walls of the plenum. The pressures at these taps are measured with a U-tube manometer or an inclined manometer, depending on the measurement range.

3. Experimental procedure

The naphthalene cassettes are prepared in a casting process. Each cassette is placed on a large, highly polished, flat, stainless steel plate with the rim of the cavity pressed against the surface of the stainless steel plate. Molten naphthalene is then poured through a hole into the cavity of the cassette. After the naphthalene solidifies, the cassette is separated from the stainless steel plate by tapping on one side of the cassette. The exposed naphthalene surface on the cassette is as flat and smooth as the surface of the highly polished stainless steel plate. To ensure that the naphthalene in all of the cassettes is in thermal equilibrium with the air in the air-conditioned laboratory for any experiment, the cassettes are stored in a sealed plastic bag in the laboratory for at least 12 h before the experiment.

To determine the average mass transfer coefficients, each naphthalene cassette is weighed before and after the experiment. The weighing process is repeated five times. The difference between the average weights gives the mass transfer from the naphthalene surface to the airflow during the experiment. The rate of mass transfer is needed to calculate the average mass transfer coefficient on the naphthalene surface.

Immediately before an experiment for determining local mass transfer coefficient distributions, each cassette is affixed onto the top platform of an x–y coordinate table, and the elevations at 27×91 pre-determined, equally spaced, grid points on the naphthalene surface of the cassette are measured with the electronic depth gauge. A desktop computer controls two stepper motors that enable the platform to transverse in two perpendicular directions in a horizontal plane. When the tip of the lever of the head of the depth gauge rests at a grid point on the naphthalene surface, the computer stops the movement of the platform momentarily and sends a voltage of 5 V to a relay switch. The relay switch triggers the amplifier of the depth gauge to transmit the elevation reading to the computer, where the reading is recorded on a spreadsheet. The automated local measurement process takes about 20 min. After the experiment, the process is repeated to obtain the elevations at the same grid points. The changes of the elevations at the grid points are used to calculate the local mass transfer coefficients.

Average and local mass transfer experiments are conducted for air flow rates corresponding to four Rey-

nolds numbers of about 7000, 14,000, 21,000, and 28,000. During each experiment, the air temperature at the test channel entrance, the pressure upstream of the orifice, and the pressure drop across the orifice are recorded every 5 min. Supplementary experiments are conducted to determine the corrections for the mass transfer from the naphthalene surfaces during blower motor startup and shutdown and due to natural convection while the naphthalene cassettes are weighed or the local elevations on the naphthalene surfaces are measured.

4. Data reduction

The Reynolds number is based on the hydraulic diameter of the test channel, D_h, and may be expressed in terms of the air mass flow rate, $\dot{m}$, the dynamic viscosity of air, μ, and the perimeter of the test channel, P.

$$Re_{D_h} = \frac{\rho \overline{V} D_h}{\mu} = \frac{4\dot{m}}{\mu P} \tag{1}$$

The overall and local mass transfer coefficients are defined, respectively, as

$$\bar{h}_m = \frac{\Delta M_n / \Delta t}{A_s(\rho_{v,w} - \bar{\rho}_{v,b})} \tag{2}$$

$$h_m = \frac{\dot{M}''_n}{\rho_{v,w} - \rho_{v,b}} = \frac{\rho_s \Delta z / \Delta t}{\rho_{v,w} - \rho_{v,b}} \tag{3}$$

where ΔM_n is the total mass transfer from a naphthalene surface to the air, Δt is the duration of the experiment, $\dot{M}''_n$ is the local naphthalene mass flux, ρ_s is the density of solid naphthalene, and Δz is the local change of elevation on the naphthalene surface. In the above equations, $\rho_{v,w}$ is the local vapor density of naphthalene at the wall, and is evaluated using the ideal gas law.

$$\rho_{v,w} = \frac{p_{v,w}}{R T_w} \tag{4}$$

In Eq. (4), the vapor pressure, $p_{v,w}$, is determined using the vapor pressure–temperature correlation for naphthalene by Ambrose et al. [8].

$$T_w \log(p_{v,w}) = \frac{a_0}{2} + \sum_{s=1}^{3} a_s E_s(x) \quad \text{with}$$
$$E_1(x) = x, \;\; E_2(x) = 2x^2 - 1, \quad \text{and}$$
$$E_3(x) = 4x^3 - 3x \tag{5}$$

where $a_0 = 301.6247$, $a_1 = 791.4937$, $a_2 = -8.2536$, $a_3 = 0.4043$, and $x = (2T_w - 574)/114$. In Eq. (5), T_w is in [K] and $p_{v,w}$ is in [N/m^2].

The average bulk vapor density of naphthalene in Eq. (2) is the average of the vapor densities at the upstream and downstream edges of the naphthalene surface being considered, and is calculated as

$$\bar{\rho}_{v,b} = \frac{1}{2}\left[\left(\frac{\dot{M}_n}{\dot{V}}\right)_{\text{upstream}} + \left(\frac{\dot{M}_n}{\dot{V}}\right)_{\text{downstream}}\right] \tag{6}$$

where $\dot{M}_n$ is the rate of total mass transfer from the upstream naphthalene surfaces, and $\dot{V}$ is the volumetric flow rate of air. The bulk vapor density is zero upstream of the first blockage since there is no naphthalene vapor in the air at the test channel inlet. Similarly, the local bulk vapor density, $\rho_{v,b}$, in Eq. (3) for determining the local mass transfer coefficient at a grid point is the rate of total mass transfer from naphthalene surfaces upstream of the grid point divided by the air volumetric flow rate.

The average and local Sherwood numbers are defined, respectively, as

$$\overline{Sh}_{D_h} = \frac{\bar{h}_m D_h}{\sigma} \tag{7}$$

$$Sh_{D_h} = \frac{h_m D_h}{\sigma} \tag{8}$$

where σ is the mass diffusion coefficient for naphthalene vapor in the air. A correlation given by Goldstein and Cho [9] is used to determine the mass diffusion coefficient.

$$\sigma = 0.0681\left(\frac{T}{298.16}\right)^{1.93}\left(\frac{1.013 \times 10^5}{p}\right) \times 10^{-4} \tag{9}$$

where σ is in [m^2/s], T is in [K], and p is in [N/m^2]. According to the analogy between heat transfer and mass transfer described in Eckert [10],

$$\frac{\overline{Nu}_{D_h}}{Nu_0} = \frac{\overline{Sh}_{D_h}}{Sh_0} \tag{10}$$

$$\frac{Nu_{D_h}}{Nu_0} = \frac{Sh_{D_h}}{Sh_0} \tag{11}$$

where the reference Nusselt number and Sherwood number are based on the Dittus–Boelter correlations [11] for a fully developed turbulent flow at the same Reynolds number through a smooth channel with the same hydraulic diameter as the test channel.

$$Nu_0 = 0.023 Re_{D_h}^{0.8} Pr^{0.4} \tag{12}$$

$$Sh_0 = 0.023 Re_{D_h}^{0.8} Sc^{0.4} \tag{13}$$

In Eqs. (12) and (13), Pr is the Prandtl number and Sc is the Schmidt number.

The friction factor is determined as

$$f = \frac{(\Delta p/\Delta x) D_h}{\rho \overline{V}^2/2} = 2\rho\left(\frac{\Delta p}{\Delta x}\right)\left(\frac{A_c}{\dot{m}}\right)^2 D_h \tag{14}$$

where $\Delta p/\Delta x$ is the pressure gradient across two successive blockages and A_c is the channel flow cross-sectional area. The experimental friction factor is normalized by

the friction factor for fully developed turbulent flow in a smooth channel, f_0, which is given as [11]

$$f_0 = [0.790\ln(Re_{D_h}) - 1.64]^{-2} \quad (15)$$

The estimation of uncertainty values is based on a confidence level of 95% (or 20:1 odds) and the relative uncertainty analysis method of Coleman and Steele [12]. Also, in all uncertainty calculations, uncertainty values of ±1.0% for all properties of air and ±0.25 mm for all physical dimensions are used.

The uncertainty of the air mass flow rate is calculated from the measured values of the pressures at the orifice flow meter, and is found to be 2.91%. Using an uncertainty value of ±0.30% for the perimeter of the test channel, the maximum uncertainty of the calculated Reynolds number is ±3.09%.

With a maximum uncertainty value of ±0.4 °C for T_w, the uncertainty of $p_{v,w}$ is calculated to be ±4.0%. This value leads to an uncertainty value of ±4.94% of $(\rho_{v,w} - \rho_{v,b})$ for the vapor pressure at the naphthalene surface, $\rho_{v,w}$. Based on the local and overall mass transfer measurements, the uncertainty value for $\rho_{v,b}$ is calculated to be ±0.078% of $(\rho_{v,w} - \rho_{v,b})$, and that for $\bar{\rho}_{v,b}$ is calculated to be ±0.075% of $(\rho_{v,w} - \bar{\rho}_{v,b})$. Using uncertainty values of ±1.0% for the density of solid naphthalene, $\pm 2.5 \times 10^{-3}$ mm for Δz, and ±5.0 s for Δt, the uncertainty of the local mass transfer coefficient is estimated to be ±6.33%. Similarly, using uncertainty values of ±1.0 mg for ΔM_n and ±5.0 s for Δt, the uncertainty of the average mass transfer coefficient is estimated to be ±5.06%.

According to Goldstein and Cho [9], the diffusion coefficient of naphthalene vapor in air has an uncertainty of about ±5.0%. With this value, the calculated values of the relative uncertainties for the local and average Sherwood numbers are ±8.21% and ±7.27%, respectively.

Using the maximum uncertainty values of ±4.04% for the measured pressure drops across the blockages and ±2.91% for the air mass flow rate, the maximum value of the relative uncertainty of the friction factor is calculated to be ±7.76%.

5. Presentation and discussion of results

5.1. Average heat (mass) transfer and overall pressure drop

For turbulent air flows through four blockages with staggered holes in an 8:1 rectangular channel, average and local heat (mass) transfer and overall pressure drop results were obtained for blockages with round holes and square holes, and for four airflow rates, with corresponding Reynolds numbers, Re_{D_h}, of about 7000, 14,000, 21,000 and 28,000. The average heat (mass) transfer coefficients for three channel wall segments between consecutive blockages are given here first, along with the overall pressure drops across consecutive blockages. The results are presented as average Sherwood number or Nusselt number ratios, $\overline{Sh}_{D_h}/Sh_0$ or $\overline{Nu}_{D_h}/Nu_0$, and friction factor ratios, f/f_0.

The values of the average Sherwood number, $\overline{Sh}_{D_h}$, were first calculated based on the overall mass transfer measurements, and then based on the local elevation measurements (by taking the average of the local mass transfer coefficients on each mass transfer active surface). Corresponding values of $\overline{Sh}_{D_h}$ based on overall and local measurements were found to differ by an average of 1.91% and a maximum of less than 7.83%. Considering that the estimated uncertainties of the local and average Sherwood numbers are ±8.21% and ±7.27%, respectively, and local elevations were measured at discrete points on each naphthalene surface but not at the two ends of the surface near the side walls of the channel, the differences between these $\overline{Sh}_{D_h}$ values are quite acceptable.

Figs. 4 and 5 give $\overline{Sh}_{D_h}/Sh_0$ (or $\overline{Nu}_{D_h}/Nu_0$) as a function of Re_{D_h}, for flows through blockages with round holes and square holes, respectively. Different symbols are used in the two figures for $\overline{Sh}_{D_h}/Sh_0$ (or $\overline{Nu}_{D_h}/Nu_0$) based on overall measurements and local elevation measurements. For the blockages with round and square holes considered, $\overline{Sh}_{D_h}/Sh_0$ (or $\overline{Nu}_{D_h}/Nu_0$) decreases by up to 15.1% as Re_{D_h} is increased from 7000 to 28,000. The blockages with round holes cause higher heat (mass) transfer enhancement than the blockages with square holes, with $\overline{Sh}_{D_h}/Sh_0$ (or $\overline{Nu}_{D_h}/Nu_0$) values between 5.04 and 6.33 for round holes compared with values between 4.70 and 5.71 for square holes. These heat (mass) transfer enhancement ranges are comparable to those reported in Moon and Lau [7] for air flows through two blockages with staggered round holes that have geometries different from those in this study. Moon and Lau [7] conducted experiments using both the

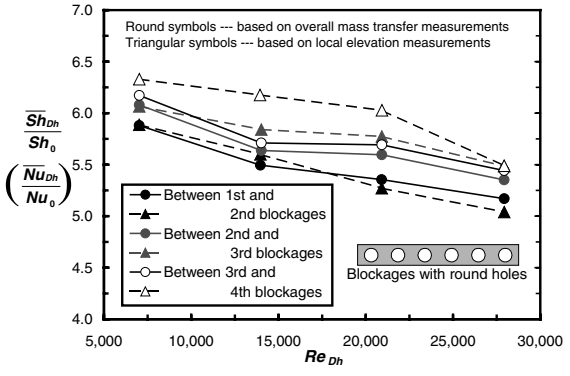

Fig. 4. Average heat (mass) transfer enhancement for flows through blockages with round holes in a rectangular channel.

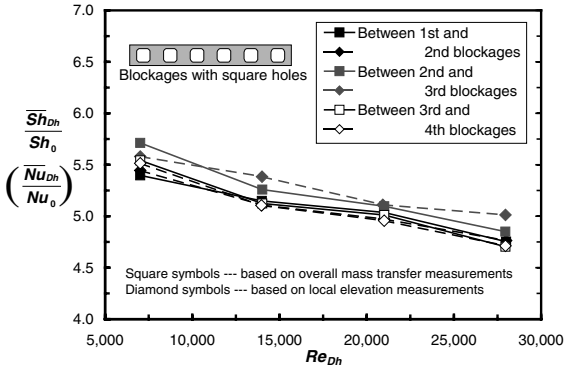

Fig. 5. Average heat (mass) transfer enhancement for flows through blockages with square holes in a rectangular channel.

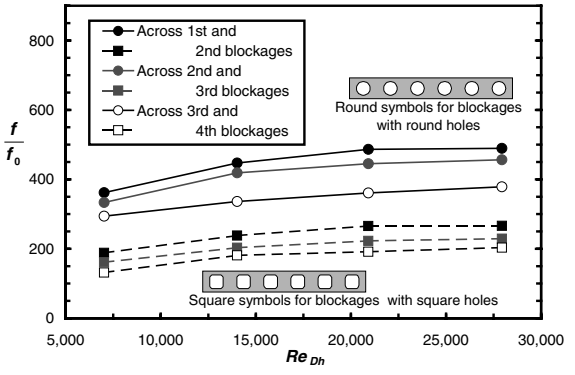

Fig. 6. Overall increases of pressure drop for flows through blockages with round and square holes in a rectangular channel.

steady liquid crystal technique and the conventional heat transfer method with electric heaters and thermocouples, and obtained overall heat transfer enhancement ranging from 4.6 to 8.1 for blockages with round holes of two sizes and nine different configurations.

For blockages with round holes, the overall heat (mass) transfer is the highest on the channel wall between the third and fourth blockages and the lowest between the first and second blockages. However, the difference between the largest and the smallest $\overline{Sh}_{D_h}/Sh_0$ (or $\overline{Nu}_{D_h}/Nu_0$) values at any Re_{D_h} is only 13.4%. For blockages with square holes, the overall heat (mass) transfer is slightly higher on the channel wall between the second and third blockages than between the first and second blockages and between the third and the fourth blockages, with a maximum variation of 6.36%.

The friction factor is defined based on the pressure drop across two consecutive blockages: the difference between the average of the static pressures at the taps upstream of a blockage and the average of the pressures at the taps downstream of the next downstream blockage. Fig. 6 presents the variation of f/f_0 with Re_{D_h} for both blockages with round and square holes. The friction factor ratio increases slightly with a decreasing slope as the Reynolds number is increased. Blockages with round holes cause larger pressure drops than blockages with square holes, which has a 27% larger flow cross-sectional area. The f/f_0 values are between 294.1 and 489.5 for blockages with round holes, and between 131.6 and 266.3 for blockages with square holes. Thus, the blockages significantly increase the pressure drop along the test channel, by up to almost 500 times that for fully developed turbulent flow through a smooth channel with the same hydraulic diameter. For both round and square holes, the friction factor ratio is the highest across the first two blockages and the lowest across the last two blockages.

Because of the very large pressure drops caused by the blockages, the values of the thermal performance ratio, defined as $(\overline{Nu}_{D_h}/Nu_0)(f/f_0)^{-1/3}$, in most cases are less than 1.0. That is, the heat transfer per unit pumping power is lower with the blockages than without them. Fig. 7 shows that, for blockages with round holes, the thermal performance ratio ranges from 0.66 to 0.93, and for blockages with square holes, the ratio ranges from 0.74 to 1.09. These ranges are comparable with those presented in Moon and Lau [7]. Fig. 8 is a plot of $\overline{Sh}_{D_h}/Sh_0$ (or $\overline{Nu}_{D_h}/Nu_0$) versus f/f_0 showing that, while the blockages with round holes enhance more heat (mass) transfer than the blockages with square holes, the blockages with round holes also cause significantly higher pressure drops, resulting in the lower thermal performance of the blockages with round holes.

In this study, the blockages with round and square holes reduce the flow cross-sectional area by 73.8% and 66.8%, respectively. Although the blockages enhance the heat (mass) transfer on the walls of the channel, the significantly reduced flow cross sections cause very large pressure drops across the blockages, resulting in the

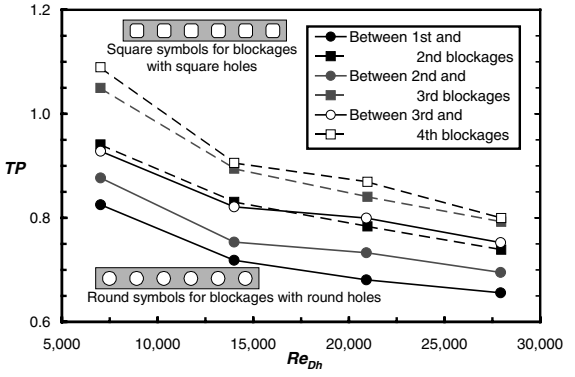

Fig. 7. Relative thermal performances for flows through blockages with round and square holes in a rectangular channel.

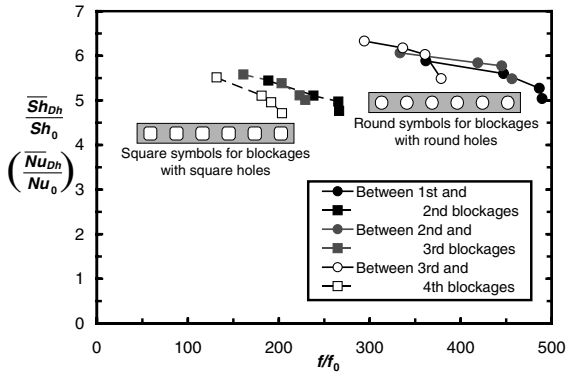

Fig. 8. Average heat (mass) transfer enhancement versus overall increase of pressure drop for flows through blockages with round and square holes in a rectangular channel.

relatively low thermal performances. The thermal performance may be improved with hole configurations that cause lower pressure drops while maintaining relatively high heat transfer enhancement on the channel walls. Further research is needed to optimize the hole configuration and the spacing between blockages to give the highest thermal performance for heat transfer enhancement on the channel walls between blockages.

The local heat (mass) transfer results, to be presented in the next section, indicate that the local heat transfer on the channel walls is very high immediately upstream of a blockage, as a result of the deflection of the air flow toward the channel walls after it impinges onto the upstream face of the blockage. Thus, the heat transfer may be much higher on the upstream face of a blockage than on the channel walls. Since the surface area of the upstream face of a blockage is a significant fraction of the exposed surface area of each wall (about one-third, for the hole and blockage configurations considered in this study) and a substantial amount of heat may be conducted from the channel wall to the blockage, the overall heat transfer may be much higher than the heat transfer from the exposed surface of the channel wall only. The values of the thermal performance ratio, presented in Fig. 7, are based on the heat transfer from the exposed surface of the channel wall only, and may be higher if the heat transfer from the surfaces of the blockages is included.

5.2. Local heat (mass) transfer distribution

Attention is now focused on the local heat (mass) transfer results. Local heat (mass) transfer coefficients were determined at a grid of 2275 (25×91) points on each of three naphthalene surfaces between consecutive blockages in a rectangular channel, except over a 0.35-cm wide region of each surface near each side wall. Local elevations were measured at these points (and points on the top of the aluminum rim of the naphthalene surface, to facilitate the calculations of the elevation changes at the points) for the same blockages with round holes and square holes, and the same four Reynolds numbers of about 7000, 14,000, 21,000, and 28,000, as for the overall mass transfer measurements.

In Figs. 9 and 10, the local heat (mass) transfer results are presented, for blockages with round holes and square holes, respectively, as contours of the local Sherwood number or Nusselt number ratio, Sh_{D_h}/Sh_0 or Nu_{D_h}/Nu_0. In these figures, arrows indicate the direction of the main flow through the test channel, and the unshaded portions of the blockages indicate the locations of the holes.

As shown in Fig. 9, for airflow through blockages with round holes, the local heat (mass) transfer is very high immediately upstream of a blockage, but is quite low immediately downstream of a blockage. After the air flows through the holes in a blockage, it impinges onto the upstream face of the downstream blockage with staggered holes. The air is then deflected toward the top and bottom channel walls, causing the very high local heat (mass) transfer immediately upstream of the blockage, with Sh_{D_h} (or Nu_{D_h}) values as high as nine

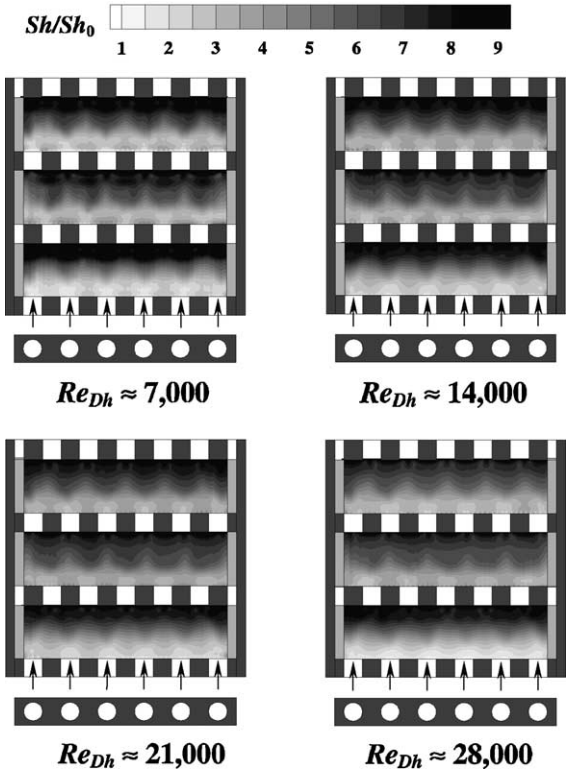

Fig. 9. Distributions of local Sherwood number ratio on wall segments for flows through blockages with round holes in a rectangular channel.

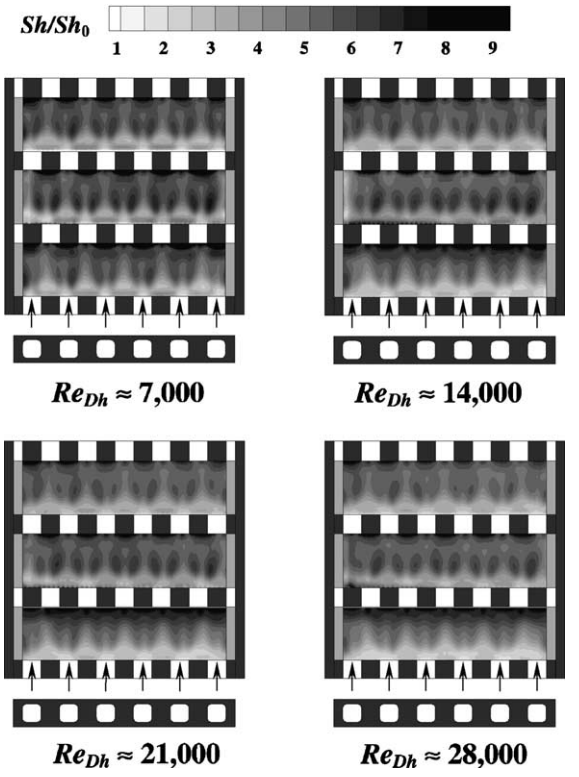

Fig. 10. Distributions of local Sherwood number ratio on wall segments for flows through blockages with square holes in a rectangular channel.

times that for fully developed flow through a smooth channel. Immediately downstream of a blockage, the flow field near the channel wall appears to be dominated by relatively slow moving recirculating flow over the channel wall. The local heat (mass) transfer is especially low immediately downstream of a hole, with values of Sherwood number (or Nusselt number) only slightly higher than that for fully developed flow through a smooth channel.

The airflow through the staggered round holes in the blockages causes a periodic spanwise Sh_{D_h}/Sh_0 (or Nu_{D_h}/Nu_0) distribution, with wavy contours occupying the middle of each wall segment between consecutive blockages, higher values immediately upstream of a blockage between two holes than upstream of a hole, and lower values downstream of a hole than downstream of a blockage between two holes. The spanwise variation of the local heat (mass) transfer coefficient, however, is small compared with the streamwise variation between blockages. The aforementioned deflected airflow toward the channel wall upstream of a blockage between two holes may turn to either side along the wall. The air may then turn away from the wall before escaping through one of the two holes. A portion of the deflected airflow may turn upstream along the wall and is drawn into the recirculation zones between the air jets passing through the holes in the upstream blockage and the wall.

There does not appear to be any reattachment of the air jets that pass through the round holes in the blockages. The air jets may reattach near the downstream end of the wall segment between two blockages where the heat (mass) transfer is very high as a result of the deflection of the flow toward the wall. For $Re_{D_h} \approx 7000$, distinctive high Sh_{D_h}/Sh_0 (or Nu_{D_h}/Nu_0) regions upstream of a blockage, in addition to the very high heat (mass) transfer region immediately upstream of a blockage, may indicate flow reattachment.

For a given air flow rate, the variation of the local heat (mass) transfer coefficient is the largest on the wall segment between the first two blockages with round holes, and is the lowest between the second and third blockages. The local heat (mass) transfer coefficient is clearly lower immediately downstream of the first blockage than downstream of the second and third blockages. The local heat (mass) transfer coefficient immediately upstream of the second blockage is higher than, or as high as, that upstream of the third and fourth blockages. The differences among the heat (mass) transfer distributions on the three wall segments between blockages may be the results of the airflow approaching the first blockage from a short open channel and exiting the last blockage into a large plenum. Because of the low local heat (mass) transfer coefficient immediately downstream of the first blockage, the average heat (mass) transfer coefficient is the lowest on the wall segment between the first two blockages (see Fig. 4).

The local heat (mass) transfer distributions for blockages with square holes, given in Fig. 10, are different from those for blockages with round holes, although they have several of the features of the distributions for blockages with round holes. The Sherwood number (or Nusselt number) ratio is high immediately upstream of a blockage and is low immediately downstream of a blockage. The streamwise variation of the local heat (mass) transfer coefficient appears to be the largest again on the wall segment between the first two blockages. There is again a periodic spanwise Sh_{D_h}/Sh_0 (or Nu_{D_h}/Nu_0) distribution, with higher values immediately upstream of a blockage between two holes than immediately upstream of a hole, and lower values downstream of a hole than downstream of a blockage between two holes.

The streamwise variation of Sh_{D_h}/Sh_0 (or Nu_{D_h}/Nu_0) over the wall segments between the blockages with square holes is smaller than that over the wall segments between blockages with round holes. With values of Sh_{D_h}/Sh_0 (or Nu_{D_h}/Nu_0) plotted using the same range between 1.0 and 9.0 in Figs. 9 and 10, it should be easy to see that the local heat (mass) transfer is not as high upstream of a blockage with square holes and not as low downstream of a blockage with square holes as in the

case of a blockage with round holes. Both the dark-colored high heat (mass) transfer regions and the light-colored low heat (mass) transfer regions are smaller in Fig. 10 than in Fig. 9. A 27% larger total flow cross-sectional area of the square holes lowers the average velocity of the flow through the holes. As a result, the flow impinges on the upstream face of the downstream blockage between the staggered holes at lower velocities.

The most significant difference between the local heat (mass) transfer distributions for blockages with square holes and for blockages with round holes is the existence of multiple distinctive high local heat (mass) transfer regions across the middle of each wall segment between blockages with square holes. The high heat (mass) transfer in these regions is the result of the reattachment on the wall of the airflow that passes through the square holes. There are two almost symmetrical reattachment regions downstream of each square hole in a blockage. The shape of the square holes, the staggered hole array, and the back flow along the wall that is deflected off the downstream blockage may all contribute to the splitting of the reattachment region downstream of each hole. Moon and Lau [7] observed flow reattachment on the wall downstream of blockages with large round holes with a diameter of 0.625 times the channel height, but no flow reattachment downstream of blockages with small round holes with a diameter-to-channel-height ratio of 0.417.

6. Concluding remarks

Naphthalene sublimation and pressure measurement experiments were conducted to study heat (mass) transfer enhancement by blockages with staggered holes for turbulent air flows in a rectangular channel. Average and local heat (mass) transfer and overall pressure drop results were obtained for blockages with round holes and square holes, and for four Reynolds numbers. The diameter of the round holes was the same as the height and the width of the square holes. For the conditions under which the experiments were conducted and the geometries of the blockages and the test channel that were studied, the results are summarized below:

- The blockages with round and square holes enhance the average heat (mass) transfer coefficients on the wall segments between the blockages by 4.7–6.3 times that for fully developed turbulent flow through a smooth channel at the same mass flow rates. The blockages with round holes enhance more heat (mass) transfer on the channel walls than the blockages with square holes, which have a 27% larger flow cross-sectional area.
- The blockages with round holes and square holes significantly increase the pressure drop along the test channel, by up to almost 270 and 490 times, respectively, that for fully developed turbulent flow through a smooth channel at the same mass flow rates.
- For a given pumping power, the blockages with square holes enhance more heat (mass) transfer on the channel wall than the blockages with round holes. Because of the very large pressure drops caused by both the blockages with round holes and square holes, the heat (mass) transfer per unit pumping power is lower with the blockages than without them. Further research is needed to optimize the hole configuration and the spacing between blockages to give the highest thermal performance for heat (mass) transfer enhancement on the channel walls between blockages.
- The local heat (mass) transfer is very high immediately upstream of a blockage, but is quite low immediately downstream of a blockage. The streamwise variation of the heat (mass) transfer coefficient on the wall segment between blockages is much larger than the spanwise variation.
- The streamwise variation of the heat (mass) transfer coefficient is smaller over the wall segment between two blockages with square holes than between two blockages with round holes.
- The air jets that pass through the square holes in a blockage reattach on the wall segment between the blockages. The flow reattachment increases the heat (mass) transfer over two symmetrical regions on the wall segment downstream of each hole. In the case of the round holes, the air jets may reattach near the downstream end of the wall segment between two blockages where the heat (mass) transfer is very high as a result of the deflection of the flow toward the wall.

Acknowledgement

Siemens-Westinghouse Power Company sponsored this research.

References

[1] J.C. Han, S. Dutta, S.V. Ekkad, Gas Turbine Heat Transfer and Cooling Technology, Taylor and Francis, New York, NY, 2000.
[2] S.C. Lau, Enhanced internal cooling of gas turbine airfoils, in: B. Sunden, M. Faghri (Eds.), Heat Transfer in Gas Turbines, WIT Press, Southampton, UK, 2001, pp. 109–173.
[3] R.T. Kukreja, S.C. Lau, Distributions of local heat transfer coefficient on surfaces with solid and perforated ribs, J. Enhanced Heat Transfer 5 (1) (1998) 9–21.
[4] J.J. Hwang, T.Y. Lia, T.M. Liou, Effect of fence thickness on pressure drop and heat transfer in a perforated-fenced channel, Int. J. Heat Mass Transfer 41 (4–5) (1998) 811–816.

[5] T.M. Liou, S.H. Chen, Turbulent heat and fluid flow in a passage distributed by detached perforated ribs of different heights, Int. J. Heat Mass Transfer 41 (12) (1998) 1795–1806.
[6] J.M. Buchlin, Convective heat transfer in a channel with perforated ribs, Int. J. Thermal Sci. 41 (2002) 332–340.
[7] S.W. Moon, S.C. Lau, An experimental study of local heat transfer distribution between blockages with holes in a rectangular channel, ASME Paper No. IMECE2002-33673, 2002.
[8] D. Ambrose, I.J. Lawrenson, C.H.S. Sprake, The vapor pressure of naphthalene, J. Chem. Thermodyn. 7 (1975) 1172–1176.
[9] R.J. Goldstein, H.H. Cho, A review of mass transfer measurements using naphthalene sublimation, Exp. Thermal Fluid Sci. 10 (1995) 416–434.
[10] E.R.G. Eckert, Analogies to heat transfer processes, in: E.R.G. Eckert, R.J. Goldstein (Eds.), Measurements in Heat Transfer, Hemisphere Publishing Corp., New York, NY, 1976, pp. 397–423.
[11] F.P. Incropera, D.P. DeWitt, Fundamentals of Heat and Mass Transfer, 5th ed., John Wiley & Sons, New York, NY, 2002.
[12] H.W. Coleman, W.G. Steele, Experimentation and Uncertainty Analysis for Engineers, John Wiley & Sons, New York, NY, 1989.